PTEP

Prog. Theor. Exp. Phys. **2025** 033G01 (16 pages)
DOI: 10.1093/ptep/ptaf031

Theoretical Study of Mismatch-Induced Halo Formation from an Intense Hadron Bunch in a Uniform Focusing Channel

Kimihiro Kato and Hiromi Okamoto *

Graduate School of Advanced Science and Engineering, Hiroshima University, 1-3-1 Kagamiyama, Higashi-Hiroshima 739-8530, Japan

Received December 4, 2024; Revised January 29, 2025; Accepted February 14, 2025; Published February 17, 2025

A basic mechanism of halo formation in high-intensity hadron accelerators is explored theoretically. As a possible origin of halos, we focus on the deviation of an initial bunch size from its ideal dimensions, in other words, spatial mismatch of the bunch shape to an accelerator lattice. Such an error is unavoidable in any machine and thus needs to be considered carefully. Assuming an axisymmetric uniform beam-focusing potential, we calculate the transverse and longitudinal wavenumbers of linear collective modes from the 3D envelope equations. The obtained analytical formulas are found to explain the power spectra derived from self-consistent numerical simulations. Approximate conditions of possible resonances driven by mismatch-induced envelope oscillation are presented to estimate dangerous parameter ranges where a particularly serious halo may develop. A simple measure to separate tail particles from the beam core is introduced, which suggests the existence of two distinct regimes of halo formation. The maximum extent of a halo as well as emittance growth rates are evaluated through systematic simulations as a function of initial mismatch factors.

Subject Index G10, G11

1. Introduction

The minimization of beam loss is imperative in modern hadron accelerators aiming at high-intensity and high-power beam generation. The loss rate must be very low in such machines to avoid radioactivation of the vacuum chamber. As the loss occurs in the beam tail (halo), it is important to understand the physical processes and conditions of halo formation. While a number of possible mechanisms of halo formation have been suggested or confirmed already (see e.g. Ref. [1] for a concise summary), we can say, after all, that halos are developed as a consequence of beam instability. The most common instability that may eventually lead to a serious halo in both linear and circular machines is the *resonance* driven either by the natural Coulomb self-field (SF-driven resonance) or by external fields from electromagnetic components (EF-driven resonance) [2–4]. Even if the external driving force is completely linear, resonances of the third and higher orders can take place in the former case because the Coulomb potential contains various nonlinear driving terms. In the latter case, lattice imperfections and correction magnets are responsible for nonlinear resonance excitation.

The resonant beam instability can be classified into two categories, in terms of its physical mechanism rather than its driving source [5–8]; one is the *coherent* type, and the other the *incoherent* type. Once the coherent resonance mechanism is activated, the motions of all or

*okamoto@sci.hiroshima-u.ac.jp

some of the core particles become unstable collectively due to strong Coulomb interaction. The Coulomb self-field potential can also be a source of incoherent resonances on which the stability of individual particles is affected almost independently. The incoherent mechanism is effective only in the beam-tail region where direct Coulomb coupling among individual particles is weak [5–7]. This picture is the theoretical basis of the so-called "particle–core model" proposed for the study of halo properties [9, 10] (see also Ref. [11] and references therein). The original instability mechanism resulting in halo formation is, however, not necessarily incoherent. In some cases, the halo formation process is triggered by coherent instability that destroys the core and, as a result, produces the seeds of a halo. The motions of those particles having escaped from the core are nearly independent and, therefore, describable within the framework of incoherent dynamics.

The resonant instability caused by lattice periodicity is avoidable by choosing a proper operating point of the accelerator, no matter whether it is SF-driven or EF-driven, coherent or incoherent. A simple guideline has been recently established to find resonance-free regions in the tune diagram [7,12,13]. In a spatially uniform transport channel, resonant instabilities are much less effective as long as the beam is well matched to the time-independent external potential. An important question now is what happens when the beam is strongly mismatched to the uniform lattice. In fact, a certain degree of mismatch is inevitable at injection in any real machine. A strong mismatch causes the beam core to execute large collective oscillation. The space-charge potential of the core then varies periodically, turning into a driving source of resonances. The purpose of the present theoretical study is to elucidate the role of this mismatch-induced core oscillation in the halo formation process. Since we are not interested in lattice-induced resonances, the external beam-focusing force is assumed to be spatially uniform. The instability studied here is thus purely SF-driven, while the driving mechanism can be either coherent or incoherent.

The paper is organized as follows. In Section 2, we derive a formula for calculating the wavenumbers of linear collective modes in a spheroidal bunch, solving the root-mean-squared (rms) envelope equations perturbatively. The conditions of possible resonances excited by core oscillation are given in Section 3. After introducing an approximate way to separate halo particles from the core in Section 4, we perform self-consistent multiparticle simulations in Section 5 and compare the results with theoretical expectations. Some concluding remarks are finally made in Section 6.

2. Envelope oscillation modes

The 3D stability of linear coherent modes against perturbation was studied in detail by Qiang, who numerically solved the envelope equations for an intense hadron bunch traveling in a periodic lattice [14]. When the lattice is uniform as assumed here, the mathematical procedure for finding the oscillation frequencies of the linear modes gets simplified considerably. Consider an axisymmetric bunch whose transverse and longitudinal rms emittances are $\varepsilon_\perp$ and $\varepsilon_\parallel$, respectively. The rms beam sizes (a, b) in the two directions obey the envelope equations

$$\frac{d^2a}{ds^2} + k_\perp^2 a - \frac{\varepsilon_\perp^2}{a^3} - I_p a \int_0^\infty \frac{dt}{(a^2+t)^2(b^2+t)^{1/2}} = 0, \tag{1a}$$

$$\frac{d^2b}{ds^2} + k_\parallel^2 b - \frac{\varepsilon_\parallel^2}{b^3} - I_p b \int_0^\infty \frac{dt}{(a^2+t)(b^2+t)^{3/2}} = 0, \tag{1b}$$

where I_p is a constant proportional to the total number of particles in the bunch, and the independent variable s represents the path length along the designed beam orbit. The focusing-strength parameters $(k_\perp,\ k_\parallel)$ correspond directly to the transverse and longitudinal bare tunes. The phases of the betatron and synchrotron oscillations advance by $k_\perp L$ and $k_\parallel L$ over the distance L at zero intensity. Since the lattice periodicity has been smoothed out, the ideal beam sizes (a_0, b_0) in the stationary state are constant and satisfy

$$(k_\perp \eta_\perp)^2 a_0 - \frac{\varepsilon_\perp^2}{a_0^3} = 0, \quad (k_\parallel \eta_\parallel)^2 b_0 - \frac{\varepsilon_\parallel^2}{b_0^3} = 0, \tag{2}$$

where $(\eta_\perp, \eta_\parallel)$ are the transverse and longitudinal tune depressions defined by

$$\eta_\perp^2 = 1 - \frac{I_p}{(k_\perp a_0)^2 b_0} F_\perp(\zeta) \quad \text{and} \quad \eta_\parallel^2 = 1 - \frac{I_p}{(k_\parallel b_0)^2 b_0} F_\parallel(\zeta). \tag{3}$$

$F_\perp(\zeta)$ and $F_\parallel(\zeta)$ are dimensionless functions of the aspect ratio $\zeta \equiv a_0/b_0$ and are expressed, for a nonspherical bunch $(\zeta \neq 1)$, as

$$F_\perp(\zeta) = \frac{1}{1-\zeta^2}\left[1 - \frac{\zeta^2}{2} f(\zeta)\right] \quad \text{and} \quad F_\parallel(\zeta) = \frac{1}{\zeta^2 - 1}\left[2 - f(\zeta)\right], \tag{4}$$

where

$$f(\zeta) = b_0 \int_0^\infty \frac{dt}{\left(a_0^2 + t\right)\left(b_0^2 + t\right)^{1/2}} = \begin{cases} -\frac{1}{\sqrt{1-\zeta^2}} \log\left|\frac{1-\sqrt{1-\zeta^2}}{1+\sqrt{1-\zeta^2}}\right| & \text{for } \zeta < 1 \\ \frac{2}{\sqrt{\zeta^2-1}}\left[\frac{\pi}{2} - \arctan\frac{1}{\sqrt{\zeta^2-1}}\right] & \text{for } \zeta > 1 \end{cases}.$$

For a spherical beam $(\zeta = 1)$, we have $F_\perp(\zeta) = F_\parallel(\zeta) = 2/3$. The tune depression is a measure of beam density in phase space. It is close to unity at low beam density and decreases toward zero as the density becomes higher. The stationary state defined here is not necessarily in thermal equilibrium.

As proved by Sacherer [15], Eqs. (1) are insensitive to the choice of the particle distribution function, provided that the charge density maintains ellipsoidal symmetry. The parameter I_p depends only very weakly on the charge distribution in the bunch. Obviously, there are two collective modes that possess ellipsoidal symmetry; one is in-phase with respect to the oscillations of a and b (breathing mode) and the other out-of-phase (quadrupole-like mode). The wavenumbers of these modes can be estimated easily. Substituting $a = a_0 + \delta a$ and $b = b_0 + \delta b$ in Eqs. (1) and leaving only first-order terms with respect to the perturbations $(\delta a, \delta b)$, we eventually reach the coupled differential equations for a nonspherical beam,

$$\frac{d^2 \delta a}{ds^2} + k_\perp^2 M_{11} \delta a + k_\perp^2 M_{12} \delta b = 0, \tag{5a}$$

$$\frac{d^2 \delta b}{ds^2} + k_\parallel^2 M_{21} \delta a + k_\parallel^2 M_{22} \delta b = 0, \tag{5b}$$

where

$$M_{11} = 4\eta_\perp^2 + \frac{3\zeta^2 - 2}{\zeta^2 - 1}\left(1 - \eta_\perp^2\right) - \left(\frac{k_\parallel}{k_\perp}\right)^2 \frac{1}{\zeta^2 - 1}\left(1 - \eta_\parallel^2\right),$$

$$M_{12} = -\frac{\zeta}{\zeta^2 - 1}\left[1 - \eta_\perp^2 - \left(\frac{k_\parallel}{k_\perp}\right)^2 \left(1 - \eta_\parallel^2\right)\right],$$

$$M_{21} = 2\left(\frac{k_\perp}{k_\parallel}\right)^2 M_{12},$$

$$M_{22} = 4\eta_\parallel^2 + \left(\frac{k_\perp}{k_\parallel}\right)^2 \frac{2\zeta^2}{\zeta^2 - 1}\left(1 - \eta_\perp^2\right) + \frac{\zeta^2 - 3}{\zeta^2 - 1}\left(1 - \eta_\parallel^2\right).$$

The wavenumbers of the eigenmodes that obey Eqs. (5) can readily be found as follows:

$$\frac{\Omega_\pm}{k_\perp} = \sqrt{\frac{1}{2}\left\{M_{11} + \left(\frac{k_\parallel}{k_\perp}\right)^2 M_{22} \pm \sqrt{\left[M_{11} - \left(\frac{k_\parallel}{k_\perp}\right)^2 M_{22}\right]^2 + 8M_{12}^2}\right\}}. \tag{6}$$

Making use of Eq. (3) together with Eq. (4), we can write the ratio $k_\parallel/k_\perp$ of the focusing strengths as

$$\left(\frac{k_\parallel}{k_\perp}\right)^2 = \frac{1 - \eta_\perp^2}{1 - \eta_\parallel^2} \cdot \frac{2\zeta^2[f(\zeta) - 2]}{2 - \zeta^2 f(\zeta)}$$

when $\zeta \neq 1$. The right-hand side of Eq. (6) turns out to be dependent only on three parameters, namely, the aspect ratio ζ and tune depressions $(\eta_\perp, \eta_\parallel)$. Given these parameters, the emittance ratio $\varepsilon_\parallel/\varepsilon_\perp$ can also be determined uniquely: the use of Eq. (2) allows us to write

$$\left(\frac{\varepsilon_\parallel}{\varepsilon_\perp}\right)^2 = \frac{1}{\zeta^4}\left(\frac{k_\parallel}{k_\perp}\right)^2 \left(\frac{\eta_\parallel}{\eta_\perp}\right)^2 = \frac{1 - \eta_\perp^2}{1 - \eta_\parallel^2}\left(\frac{\eta_\parallel}{\eta_\perp}\right)^2 \cdot \frac{2[f(\zeta) - 2]}{\zeta^2[2 - \zeta^2 f(\zeta)]}.$$

Ω_+ corresponds to the wavenumber of the in-phase mode, Ω_- to that of the out-of-phase mode. In an extremely long bunch ($\zeta \ll 1$), we find $\Omega_+ \approx k_\perp\sqrt{2(1 + \eta_\perp^2)}$ and $\Omega_- \approx 0$. Barnard and Lund previously performed a similar perturbative analysis for a uniform ellipsoidal bunch to obtain the wavenumbers of the linear modes [16,17]. Recalling the insensitivity of Eqs. (1) to the charge distribution in the bunch, we expect that our result here should almost agree with theirs.

Figure 1 shows a few examples of $\Omega_\pm$ plotted as a function of the transverse tune depression. We have assumed an equipartitioned bunch that satisfies

$$\frac{\varepsilon_\parallel}{\varepsilon_\perp} = \frac{\eta_\perp k_\perp}{\eta_\parallel k_\parallel}, \tag{7}$$

though the present theory can generally be applied to any nonequipartitioned states. In an equipartitioned case, we only need to give two of the three fundamental parameters mentioned above; the remaining one is chosen so as to fulfill Eq. (7). The emittance ratio $\varepsilon_\parallel/\varepsilon_\perp$ of an equipartitioned bunch is equal to the aspect ratio $1/\zeta$. When the bunch is spherical ($\zeta = 1$), the eigen wavenumbers are given by $\Omega_+ = k\sqrt{3 + \eta^2}$ and $\Omega_- = k\sqrt{2(3 + 7\eta^2)/5}$ with $k_\perp = k_\parallel (\equiv k)$ and $\eta_\perp = \eta_\parallel (\equiv \eta)$. At the low-density limit, both wavenumbers converge to $2k$.

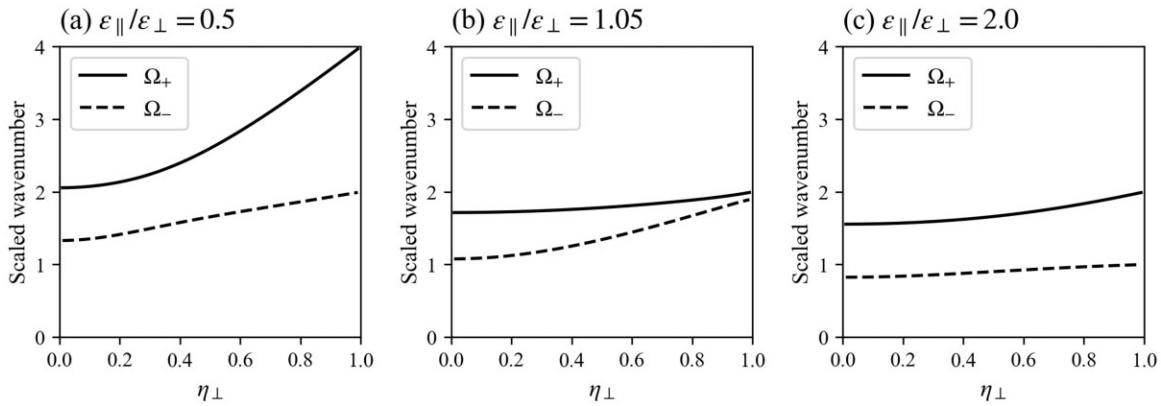

Fig. 1. Beam-density dependence of the scaled eigen wavenumbers $\Omega_\pm/k_\perp$ when the beam is equipartitioned. The emittance ratio is adjusted to (a) $\varepsilon_\parallel/\varepsilon_\perp = 0.5$, (b) $\varepsilon_\parallel/\varepsilon_\perp = 1.05$, and (c) $\varepsilon_\parallel/\varepsilon_\perp = 2.0$.

3. Possibility of parametric core resonance

The distribution of particles in real space is more and more homogenized at higher beam density due to a kind of Debye screening. Taking this fact into account, we assume a uniform spheroidal bunch here for simplicity. The bunch has a sharp boundary defined by $(x^2+y^2)/\tilde{a}^2 + z^2/\tilde{b}^2 = 1$, where $\tilde{a} = \sqrt{5}a$ and $\tilde{b} = \sqrt{5}b$. The Hamiltonian of this dynamical system can be written as

$$H = \frac{p_x^2 + p_y^2 + p_z^2}{2} + \frac{1}{2}k_\perp^2 f_\perp(\tilde{a},\tilde{b})(x^2+y^2) + \frac{1}{2}k_\parallel^2 f_\parallel(\tilde{a},\tilde{b})z^2, \tag{8}$$

where

$$f_\perp(\tilde{a},\tilde{b}) = 1 - \frac{\tilde{I}_p}{k_\perp^2}\int_0^\infty \frac{dt}{(\tilde{a}^2+t)^2(\tilde{b}^2+t)^{1/2}} \quad \text{and} \quad f_\parallel(\tilde{a},\tilde{b}) = 1 - \frac{\tilde{I}_p}{k_\parallel^2}\int_0^\infty \frac{dt}{(\tilde{a}^2+t)(\tilde{b}^2+t)^{3/2}} \tag{9}$$

with a constant intensity parameter $\tilde{I}_p$ directly linked to I_p. In the stationary state, we have $f_\perp(\sqrt{5}a_0, \sqrt{5}b_0) = \eta_\perp^2$ and $f_\parallel(\sqrt{5}a_0, \sqrt{5}b_0) = \eta_\parallel^2$.

When the beam is initially mismatched to the external focusing potential, the envelope starts to oscillate about the stationary state, so we substitute $\tilde{a}/\sqrt{5} = a_0 + \delta a$ and $\tilde{b}/\sqrt{5} = b_0 + \delta b$ in Eq. (9) assuming that the beam roughly keeps the uniform density profile. The first-order expression of $f_\perp(\tilde{a},\tilde{b})$ then takes the form $f_\perp \approx \eta_\perp^2(1 + A\delta a + B\delta b)$ with the constant coefficients A and B dependent on the beam intensity and matched envelope sizes. As shown in the last section, δa and δb oscillate at the wavenumber Ω_+ or Ω_-. The equation of the transverse particle motion derived from the Hamiltonian is, therefore, reduced to the Mathieu type,

$$\frac{d^2w}{ds^2} + k_\perp^2\eta_\perp^2[1 + D\cos(\Omega_\pm s)]w = 0, \tag{10}$$

where w stands for either x or y, and D depends on A, B, and the degree of mismatch. A similar equation can be reached for the longitudinal motion.

The solution of this Mathieu-type equation becomes unstable when the following parametric resonance conditions are met:

$$2k_\perp\eta_\perp \approx n\Omega_\pm, \tag{11a}$$

$$2k_\parallel\eta_\parallel \approx n\Omega_\pm, \tag{11b}$$

where n is an integer. The widths of these resonances are related to the parameter D. The conditions above are similar to those obtained for a coasting round beam [10] but considerably generalized to include the longitudinal dynamics and an arbitrary integer n.

We must keep in mind that the mathematical procedure leading to Eqs. (11) is not self-consistent. It is based on a sort of frozen space-charge model as the beam maintains the uniform density profile even on resonance. A single particle governed by Eq. (10) is initially inside the beam core, which conflicts with the understanding that core particles behave only coherently. Equations (11), however, provide a useful insight into the beam stability, just like the resonance condition obtained by Gluckstern from a similar analytic model [10]. As demonstrated later, the above formulas enable one to make a rough estimate of parameter ranges where the core stability is affected.

4. Defining tail particles and mismatch factors

Individual particles forming a halo execute 3D oscillation about the bunch centroid just like other particles, so we cannot perfectly separate them from core particles simply by observing the beam in real space. At any moment, a lot of halo particles are hidden behind the real-space core. Once we take a projection of the *full* phase-space distribution onto any partial space of lower dimension, some important information for halo-particle identification will be lost [7,12].

In the full phase space, 6D in the present case, we will observe halo particles staying outside the 6D beam core and moving around it. The distance of any particle from the core center is determined by its total energy in the beam frame. Particles with high total energies have large 6D amplitudes, thus forming a halo around the phase-space core. This simple picture works fine for coasting beams, giving us an easy way to identify halo particles [12]. Similarly, we here introduce the following parameter as an approximate measure of the 6D oscillation amplitudes of individual particles in a bunched beam:

$$E \equiv k_\perp \eta_\perp (J_x + J_y) + k_\parallel \eta_\parallel J_z, \tag{12}$$

where

$$2J_w = \beta_w p_w^2 + 2\alpha_w w p_w + \gamma_w w^2, \tag{13}$$

with w standing for one of the three spatial coordinates (x, y, z). α_w, β_w, and γ_w are modified Courant–Snyder functions incorporating the effect from the linear term in the Coulomb self-field potential. The accuracy of energy estimation based on this parameter will be worsened at higher beam density as we have ignored the contribution from nonlinear space-charge terms.

For the study of mismatch-induced halo formation, it is essential to define the degree of an initial mismatch precisely. The first step for this purpose is to carry out the *fine-grained matching* of an incident beam to the machine lattice in phase space. At high density, this task is not so easy because we must take the effect from the strong Coulomb potential self-consistently into account. The *rms matching* (second-moment matching) procedure, often adopted in the old days, does not work at all. As a result of the Debye screening effect mentioned above, an rms-matched beam cannot be stationary at high density; it naturally tries to approach the ideal matched state right after the injection and the resultant core oscillation gives rise to a serious halo [18,19]. Such an undesired natural effect can be considerably mitigated by the use of a pseudo-equilibrium distribution [13,20]. The rms emittance growth caused by deviation of the pseudo-equilibrium distribution from the perfect equilibrium state is less than a few percent unless the tunes are too strongly depressed. According to our past experience, the pseudo-equilibrium matching is

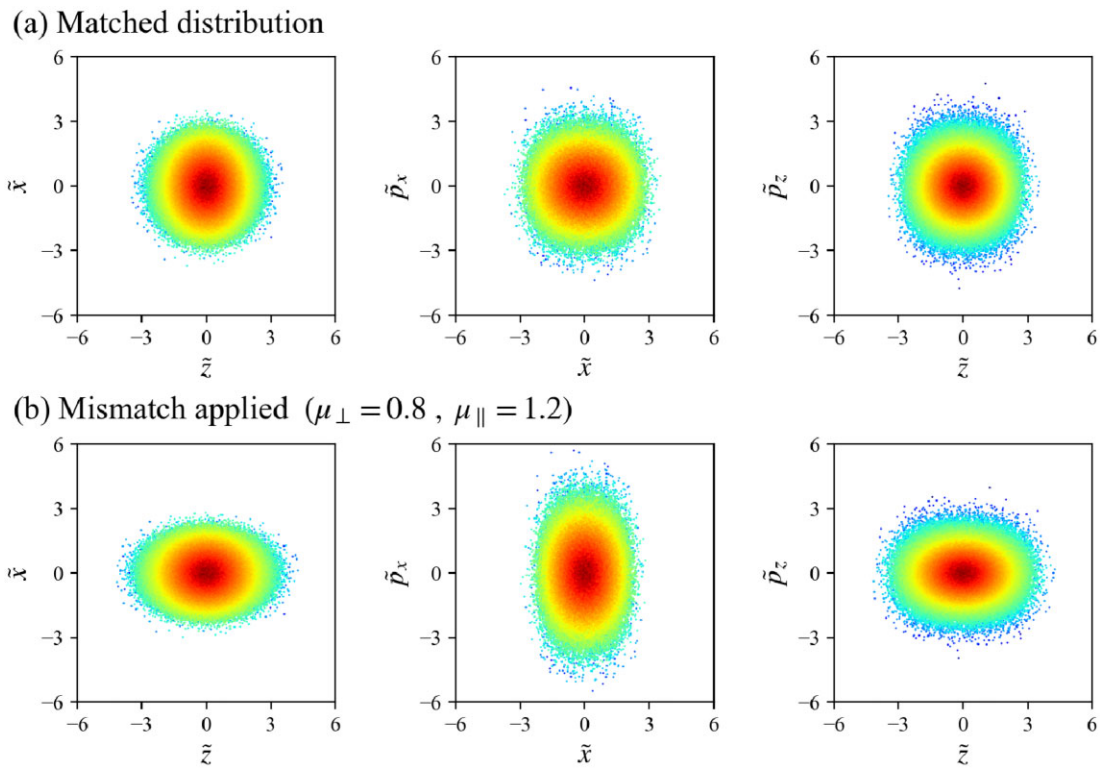

Fig. 2. Examples of Gaussian distributions at injection. The horizontal and vertical axes are canonical coordinates scaled by their rms values at injection. (a) The pseudo-equilibrium distribution of particles in real and phase spaces. The rms tune depressions are adjusted to $\eta_\perp = \eta_\parallel = 0.7$ with the emittance ratio $\varepsilon_\parallel/\varepsilon_\perp = 2.0$. (b) The particle distribution after the application of a mismatch ($\mu_\perp = 0.8$ and $\mu_\parallel = 1.2$) to the matched beam in the upper panels.

satisfactory in a range of tune depression above 0.5–0.6. A pseudo-equilibrium bunch, corresponding approximately to a stationary solution to the Vlasov–Poisson equations, should not be confused with a thermally equilibrated (equipartitioned) bunch; the former is more general, including the latter as a special case.

Once an approximate stationary state is established, it is straightforward to define the degree of an initial mismatch with no ambiguity. The following simple procedure is taken for the present numerical study. We first construct a pseudo-equilibrium distribution and calculate the E-value for each particle from Eq. (12). Spatial mismatches are then applied to the transverse and longitudinal directions independently. Since our concern here is the lowest-order axisymmetric modes, we only consider an axisymmetric mismatch at the entrance of the uniform focusing channel. The mismatch factors are defined as $\mu_\perp \equiv a_{\rm in}/a_0$ and $\mu_\parallel \equiv b_{\rm in}/b_0$ where $(a_{\rm in},\ b_{\rm in})$ are the transverse and longitudinal rms beam sizes at injection. These mismatches are introduced in such a way that the rms emittances are preserved (otherwise, the beam density in phase space is changed significantly); specifically, the transverse and longitudinal spatial coordinates of each particle are multiplied by $\mu_\perp$ and $\mu_\parallel$, the conjugate momenta by $1/\mu_\perp$ and $1/\mu_\parallel$. An example of initial beam distributions before and after the application of a mismatch is exhibited in Fig. 2. The bunch is not equipartitioned. The color of each particle is chosen based on the initial E-value defined by Eq. (12). The color varies from red to blue as the E-value increases. We see that, even in the 2D projected spaces, particles with higher energies are further from the center of the beam core.

5. Simulation results

We are now ready to look into numerical data obtained through systematic multiparticle simulations. The 3D particle-in-cell (PIC) code named "WARP" [21,22] was employed to clarify the dependence of halo properties on fundamental parameters. In all PIC simulations below, the transport distance is fixed at 200 m before which the emittance growth usually comes to a plateau under the initial conditions considered here. The bunch has a Gaussian distribution of particles initially in all three degrees of freedom. We assume low-energy (3 MeV) beams of protons that have a normalized transverse rms emittance typically of the order of $10^{-8}\,\pi\,\mathrm{m}\cdot\mathrm{rad}$ at injection. The longitudinal emittance and total number of protons in a bunch are used as free parameters to adjust the tune depressions $(\eta_\perp, \eta_\parallel)$ to target values. Note that such parameters as the mass and kinetic energy of simulation particles are physically unessential; as pointed out above, what really matters is how we set the rms tune depressions and aspect ratio (or, equivalently, the emittance ratio). Even if we choose a beam of another ion species traveling at a different energy, the time evolution of the emittance growth rate does not change at all as long as the initial tune depressions are fixed. This is true not only in the present uniform focusing model but also in any alternating-gradient channels.

5.1. *Power spectrum of mismatched envelope oscillation*

Figure 3 shows the final distributions of particles after the initially matched and mismatched beams in Fig. 2 are transported over 200 m. In the upper case (a) where the bunch has a pseudo-equilibrium distribution at injection, almost no emittance growth occurs; the final distribution

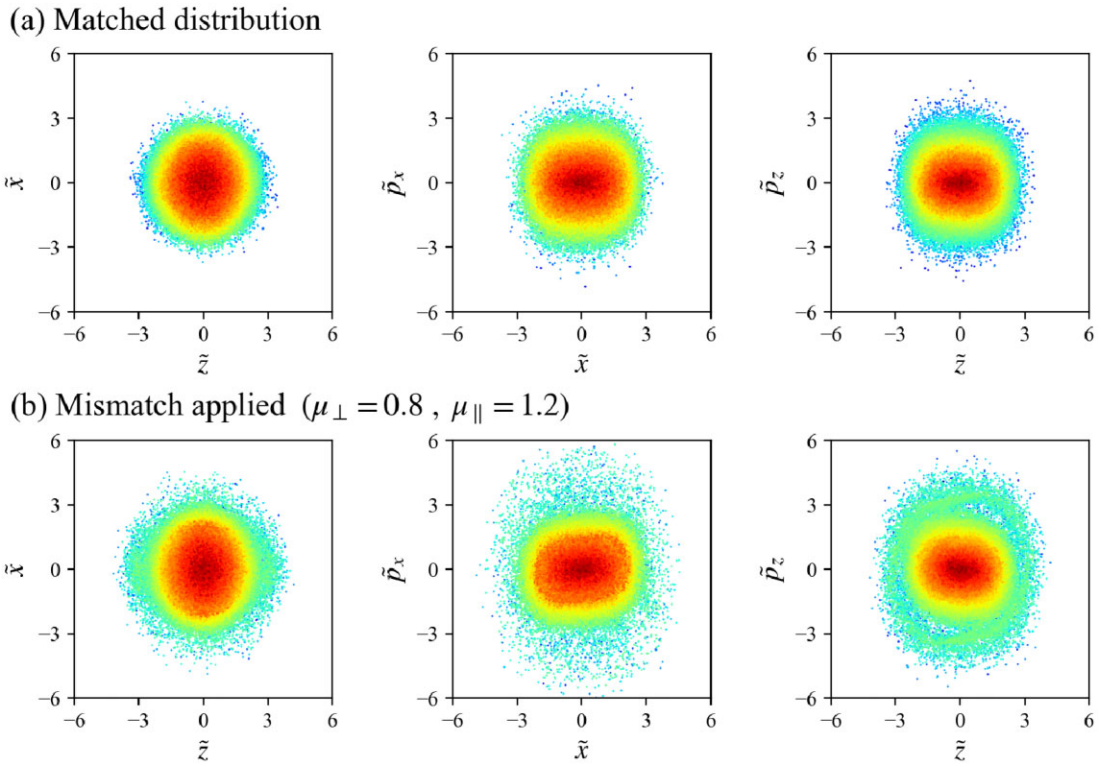

Fig. 3. Final particle distributions at the end of a long beam transport channel. The two distributions displayed in Fig. 2 have been assumed at the entrance: (a) a pseudo-equilibrium Gaussian bunch, and (b) an initially mismatched bunch with $\mu_\perp = 0.8$ and $\mu_\parallel = 1.2$.

at the transport exit looks quite similar to the initial distribution in Fig. 2(a). Slight distortion can be seen in phase space due to the incompleteness of the pseudo-equilibrium distribution, but the emittance growth is lower than 0.5%. In contrast, the bunch configuration has been seriously distorted in Fig. 3(b) by the initial mismatch applied. We observe a significant halo formed in both the transverse and longitudinal directions.

The envelope oscillation of the mismatched beam in Fig. 2(b) is Fourier analyzed to obtain the power spectrum in Fig. 4. The vertical lines in the picture indicate the values of $\Omega_{\pm}/k_{\perp}$ predicted by the formula in Eq. (6), which successfully explain the peak positions of the spectra. A few more examples with different choices of fundamental parameters are offered in Fig. 5. The theoretical prediction is still in very good agreement with the PIC data.

5.2. *Dependence on mismatch factors and tune depressions*

Emittance growth must be more severe as the initial mismatch becomes greater. Before proceeding to PIC simulations for confirmation of this natural expectation, we examine the coupled envelope motion in a bit more detail. The general solution to Eqs. (5) can be expressed as the superposition of the two coherent oscillation modes:

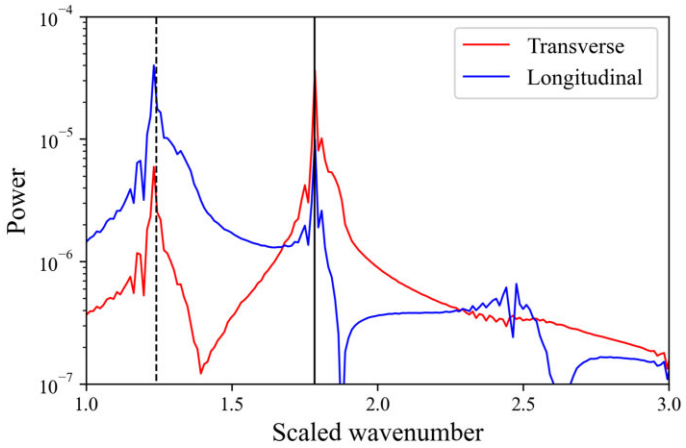

Fig. 4. Power spectra of the transverse and longitudinal envelope oscillations of the mismatched beam in Fig. 2(b). The abscissa represents the wavenumber normalized by $k_{\perp}$. The vertical solid and dashed lines indicate $\Omega_{+}/k_{\perp}$ and $\Omega_{-}/k_{\perp}$, respectively, evaluated from Eq. (6).

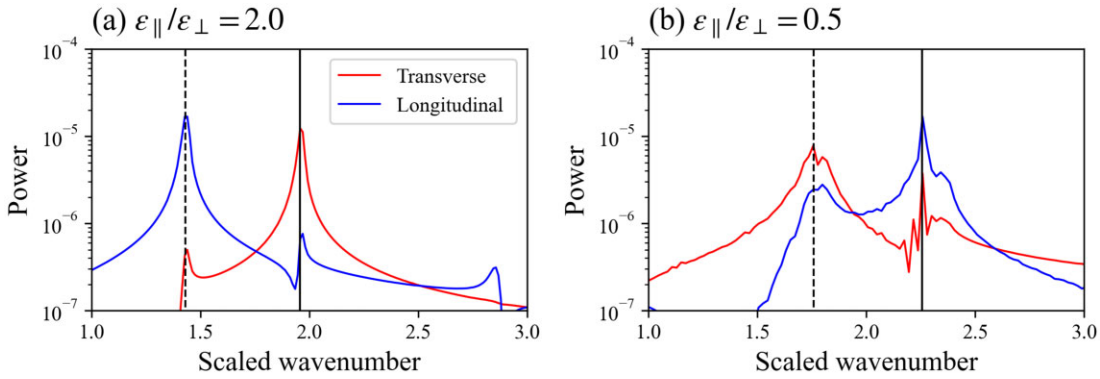

Fig. 5. Power spectra of the transverse and longitudinal rms envelope oscillations excited by an initial mismatch with $\mu_{\perp} = \mu_{\parallel} = 1.1$. Other parameters before the application of the mismatch are as follows: (a) $\varepsilon_{\parallel}/\varepsilon_{\perp} = 2.0$, $\eta_{\perp} = \eta_{\parallel} = 0.95$ and (b) $\varepsilon_{\parallel}/\varepsilon_{\perp} = 0.5$, $\eta_{\perp} = \eta_{\parallel} = 0.7$.

$$\delta a = c_+ \cos(\Omega_+ s + \varphi_+) + c_- \cos(\Omega_- s + \varphi_-), \tag{14a}$$

$$\delta b = c_+ \Gamma_+ \cos(\Omega_+ s + \varphi_+) + c_- \Gamma_- \cos(\Omega_- s + \varphi_-), \tag{14b}$$

where $c_\pm$ and $\varphi_\pm$ are integration constants, and $\Gamma_\pm = (\Omega_\pm^2 - k_\perp^2 M_{11})/k_\perp^2 M_{12}$. Let us now calculate the amplitudes $c_\pm$ corresponding to the initial conditions $\delta a(0) = (\mu_\perp - 1)a_0$, $\delta b(0) = (\mu_\parallel - 1)b_0$, and $(d\delta a/ds)_{s=0} = 0 = (d\delta b/ds)_{s=0}$. After straightforward algebra, we find

$$c_+ = \frac{\Gamma_-(\mu_\perp - 1)a_0 - (\mu_\parallel - 1)b_0}{\Gamma_- - \Gamma_+} \quad \text{and} \quad c_- = \frac{\Gamma_+(\mu_\perp - 1)a_0 - (\mu_\parallel - 1)b_0}{\Gamma_+ - \Gamma_-},$$

which suggests that one of the two collective modes may be weakened even in a mismatched beam if

$$\frac{\mu_\parallel - 1}{\mu_\perp - 1} = \begin{cases} \Gamma_- \zeta \\ \Gamma_+ \zeta \end{cases} \tag{15}$$

with $\mu_{\perp(\parallel)} \neq 1$. The upper condition in Eq. (15) comes from $c_+ = 0$ (breathing-mode suppression), the lower from $c_- = 0$ (quadrupole-mode suppression).

We carried out systematic PIC simulations to visualize how much emittance growth occurs depending on the degree of initial mismatches in the transverse and longitudinal directions. Figure 6 summarizes the results of simulations performed with about 1700 different combinations of $(\mu_\perp, \mu_\parallel)$ at a tune depression of 0.8. The left and right panels show the emittance

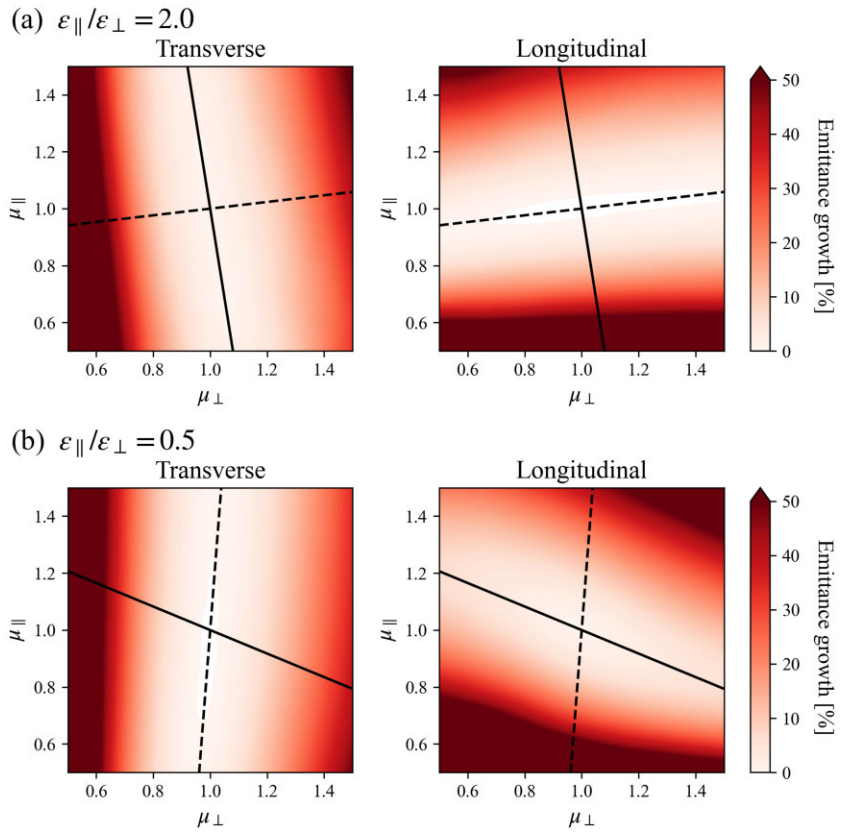

Fig. 6. Dependence of emittance growth on the mismatch factors. The rms tune depressions are fixed at $\eta_\perp = \eta_\parallel = 0.8$ initially while we have assumed an emittance ratio of $\varepsilon_\parallel/\varepsilon_\perp = 2.0$ in the upper panels (a) and $\varepsilon_\parallel/\varepsilon_\perp = 0.5$ in the lower panels (b). The solid and dashed lines are obtained from Eq. (15).

growth observed in the two directions. The emittance ratio $\varepsilon_\parallel/\varepsilon_\perp$ is adjusted initially to 2.0 in the upper panels and to 0.5 in the lower. These conditions are free from the parametric resonance in Eqs. (11). If an emittance ratio and tune depressions are chosen near that condition, emittance growth occurs almost everywhere regardless of the mismatch factors.

The PIC data in Fig. 6 indicate that severe emittance growth occurs only in the direction with a strong mismatch; at this level of beam density ($\eta_\perp = \eta_\parallel = 0.8$), the growth rate is limited in the transverse (longitudinal) direction under the condition $\mu_\perp \approx 1$ ($\mu_\parallel \approx 1$) even if the beam has a strong mismatch in the other direction. We recognize that the beam is particularly insensitive to mismatches along the lines defined by Eq. (15). The solid line corresponds to the $c_+ = 0$ case, the dashed line to the $c_- = 0$ case. When $\varepsilon_\parallel/\varepsilon_\perp = 2.0$, the transverse (longitudinal) emittance growth can be minimized by deactivating the breathing (quadrupole) mode. The roles of the two modes in emittance growth are reversed when $\varepsilon_\parallel/\varepsilon_\perp = 0.5$.

The emittance growth is naturally more enhanced at higher beam density, as shown in Fig. 7, where the tune depression has been reduced to 0.5. Other conditions are identical to the case in Fig. 6. We now observe nonnegligible emittance growth even under the condition in Eq. (15). In a strongly mismatched beam, a serious transverse (longitudinal) halo can be produced by a longitudinal (transverse) mismatch through Coulomb coupling, depending on the initial emittance ratio. Such a coupling effect has been pointed out previously by Fedotov et al. [23].

In terms of a beam-pipe design, the maximum extent of a halo, rather than emittance growth rate, is of more interest. Let us define the halo expansion rate ρ as the ratio of the maximum

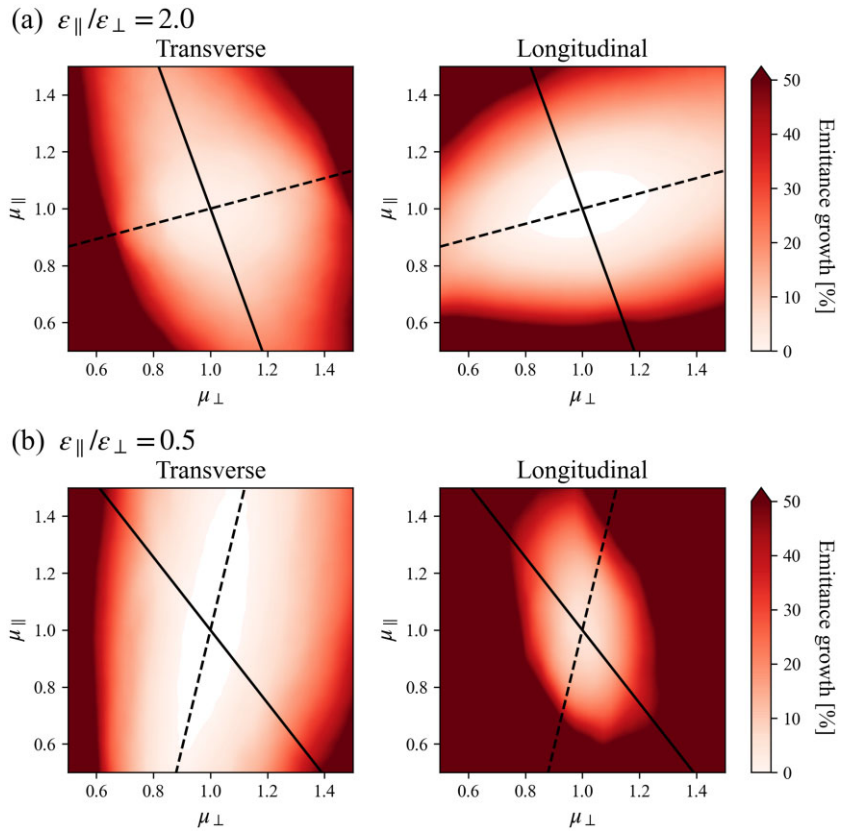

Fig. 7. Dependence of emittance growth on the mismatch factors. The rms tune depressions are fixed at $\eta_\perp = \eta_\parallel = 0.5$ with two different initial emittance ratios: (a) $\varepsilon_\parallel/\varepsilon_\perp = 2.0$ and (b) $\varepsilon_\parallel/\varepsilon_\perp = 0.5$.

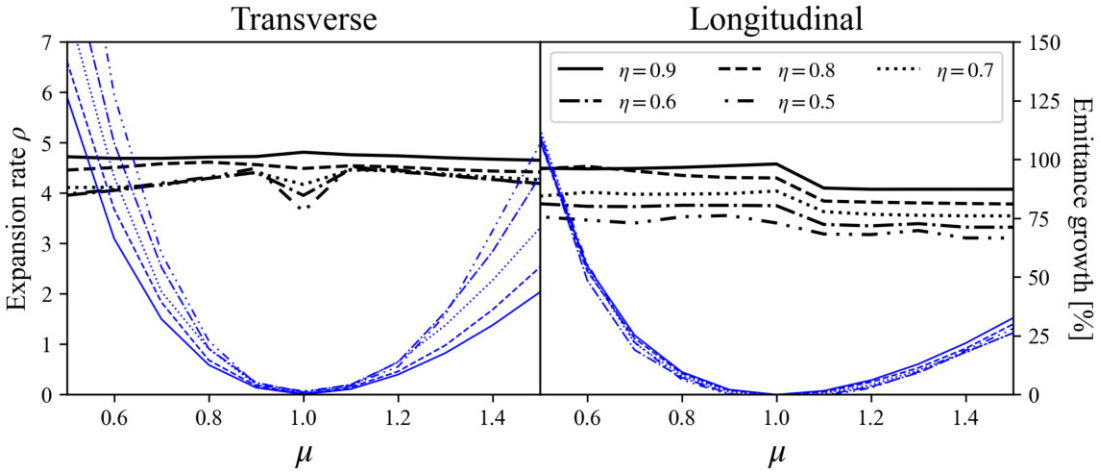

Fig. 8. Maximum halo extent vs. mismatch factor. Five different tune depressions have been taken initially with the emittance ratio fixed at $\varepsilon_\parallel/\varepsilon_\perp = 2.0$. The black lines represent the halo expansion rates $\rho_\perp$ (left panel) and $\rho_\parallel$ (right panel) evaluated at various μ values. The corresponding emittance growth is also plotted with blue lines for reference.

single-particle coordinate ($|x_{\max}|$ or $|z_{\max}|$) to the maximum rms envelope size ($a_{\max}$ or $b_{\max}$) measured during the beam transport; namely, $\rho_\perp \equiv |x_{\max}|/a_{\max}$ and $\rho_\parallel \equiv |z_{\max}|/b_{\max}$. We here consider the symmetric mismatch situation where $\mu_\perp = \mu_\parallel (\equiv \mu)$. When $\mu > 1$, $a_{\max}$ and $b_{\max}$ are almost equal to μa_0 and μb_0, respectively. In the range of $\mu < 1$, the maximum envelope size becomes somewhat greater than $2 - \mu$ times the matched rms size because of the initial bunch compression that enhances the beam density. For example, $a_{\max}$ is more than 30% larger than $(2 - \mu)a_0$ at $\mu = 0.5$.

The transverse and longitudinal expansion rates are plotted in Fig. 8 as a function of μ. The tune depression η is adjusted to a target value by changing the beam intensity (in other words, the total number of protons in a bunch, nonequipartitioned with the present parameter setup). Interestingly, $\rho_\perp$ and $\rho_\parallel$ are quite insensitive to the degree of initial mismatch; both expansion rates roughly keep a constant level over a wide range of μ. We notice that ρ tends to be slightly smaller at lower η, but this does not mean a reduction of the halo extent because the matched rms beam size grows at higher density. $|x_{\max}|$ at $\eta = 0.5$ is actually a bit larger compared with the size at $\eta = 0.9$. In any case, the beam-density dependence of ρ looks weak. $\rho_\perp$ does not exceed 4.8 within the range $0.5 < \mu < 1.5$ while $\rho_\parallel$ is always below 4.6. This observation is consistent with a previous conclusion made in Ref. [18] on coasting round beams.

5.3. *Core and tail resonances*

A previous simulation study with coasting round beams has demonstrated that a major portion of the particles forming a typical mismatch-induced halo come from the vicinity of the beam edge in phase space [18]. We expect that halos from bunched beams should have similar characteristics. In the case of Fig. 3(b), for instance, we can almost completely eliminate the halo by removing the top 20% of high-energy particles. The emittance growth evaluated from the remaining 80% of particles is at a negligible level, i.e. 1.5% in the transverse direction and 0.2% in the longitudinal. Even in the case where we disregard only the top 10% particles in the emittance evaluation, the growth rate still drops to 1.9% in the transverse direction and 3.2% in

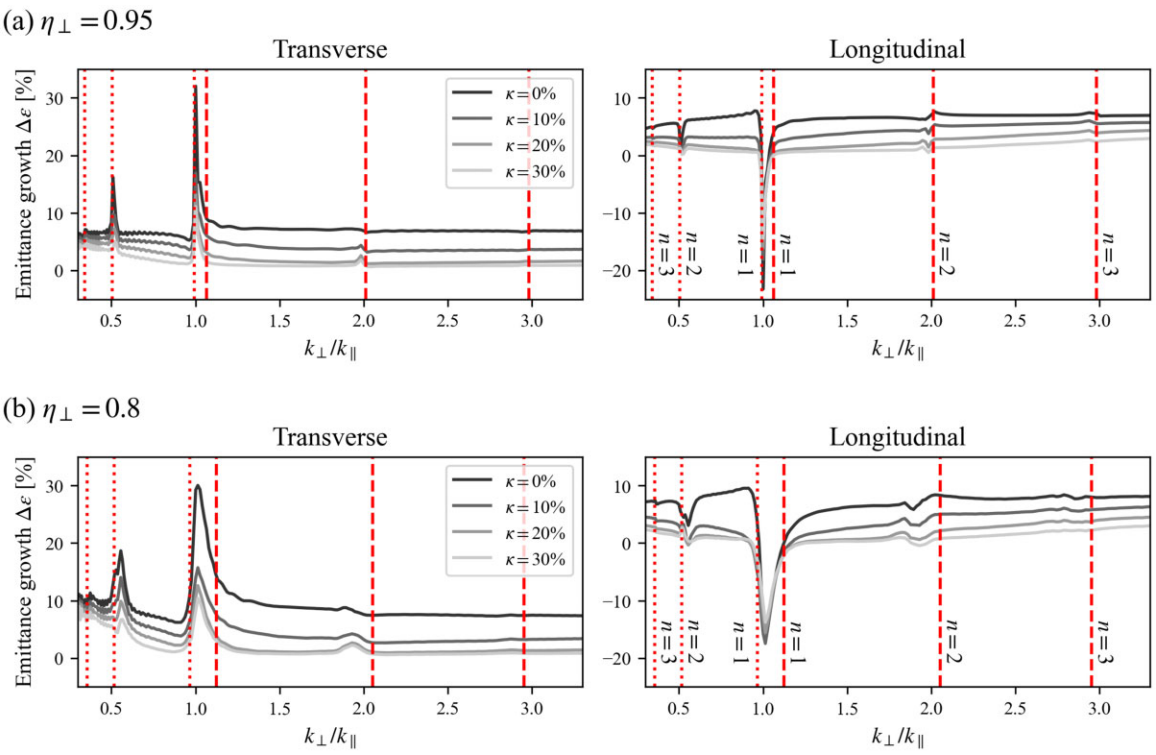

Fig. 9. Transverse and longitudinal emittance growth vs. $k_\perp/k_\parallel$ with the initial emittance ratio adjusted to $\varepsilon_\parallel/\varepsilon_\perp = 2.0$. The beam intensity has been fixed at the value that gives (a) $\eta_\perp = 0.95$ or (b) $\eta_\perp = 0.8$ when $k_\perp/k_\parallel = 1.0$. The mismatch factor is chosen to be $\mu = 1.2$ in both cases. Four curves in each picture represent the growth rates evaluated with four different percentages of tail truncation, i.e. $\kappa = 0$ % (full beam), 10%, 20%, and 30%. The vertical lines indicate where the condition in Eq. (11a) (dashed) or Eq. (11b) (dotted) is fulfilled. The number written beside each line denotes the value of n on the right-hand side of Eqs. (11). The transverse emittance growth over 5% observed near the left end ($k_\perp/k_\parallel \lesssim 1.0$) is due partially to a weak error in the pseudo-equilibrium matching.

the longitudinal. This is evidence that a typical mismatch-induced halo is formed by particles with high E-values.

The rms emittance growth rates evaluated at two different beam intensities are plotted in Fig. 9 as a function of $k_\perp/k_\parallel$. The mismatch factor assumed is $\mu = 1.2$. The ordinate is the transverse or longitudinal growth rate defined as $\Delta\varepsilon(\kappa) = [\varepsilon_{\rm out}(\kappa)/\varepsilon_{\rm in}(\kappa) - 1] \times 100$ with $\varepsilon_{\rm in}(\kappa)$ and $\varepsilon_{\rm out}(\kappa)$ denoting the rms emittances at the entrance and exit of the 200 m long beam transport line. κ represents the percentage of high-E particles that are disregarded in emittance evaluation. For instance, $\varepsilon_{\rm out}(10)$ is the final rms emittance of the tail-truncated distribution in which the top 10% of high-E particles have been removed. The final emittance of the full beam is $\varepsilon_{\rm out}(0)$. As expected, the emittance growth can be strongly suppressed over a wide range of $k_\perp/k_\parallel$ by ignoring tail particles with high E-values. We, however, discover several narrow instability bands within which particularly serious emittance growth occurs. It has been confirmed through separate simulations that the sharp emittance change near $k_\perp/k_\parallel = 1$ does not disappear even in a matched beam ($\mu = 1.0$). Such dangerous operating ranges are located near the vertical lines derived from the parametric resonance conditions in Eqs. (11). In those instability bands, the removal of high-E particles cannot be of much help to bring $\Delta\varepsilon$ close to zero, which implies that not only the beam tail but also the core have become unstable there.

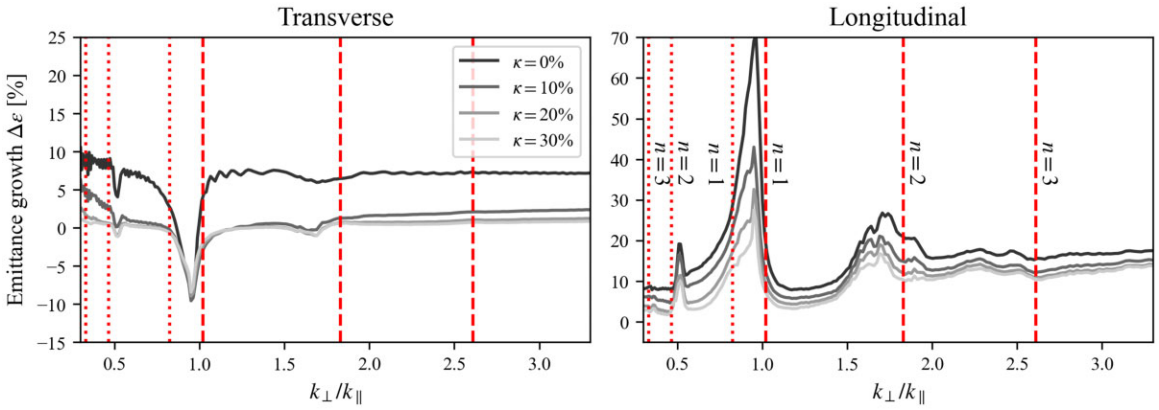

Fig. 10. Transverse and longitudinal emittance growth vs. $k_\perp/k_\parallel$ with the initial emittance ratio adjusted to $\varepsilon_\parallel/\varepsilon_\perp = 0.5$. All simulation parameters except for the initial value of $\varepsilon_\parallel/\varepsilon_\perp$ are identical to those assumed in Fig. 9(b).

All of the possible core instability bands identified in Fig. 9 are associated with the quadrupole-like modes (Ω_-); the breathing mode that has the wavenumber Ω_+ is not excited here. The emittance behavior within the parametric resonance bands indicates the presence of strong Coulomb coupling that causes an emittance exchange between the transverse and longitudinal directions. The direction of the emittance flow is quite understandable; since $\varepsilon_\parallel > \varepsilon_\perp$ at the beginning, the emittance flows from the longitudinal to the transverse direction. The PIC data obtained under the initial condition of $\varepsilon_\parallel/\varepsilon_\perp = 0.5$ are shown in Fig. 10. The direction of emittance flow has been reversed as anticipated. In the case of Fig. 10, the initial phase-space matching becomes more difficult at higher $k_\perp/k_\parallel$ because $\eta_\parallel$ decreases to the 0.5 level in the longitudinal direction. This should be a primary reason for the gradual longitudinal emittance growth in a high $k_\perp/k_\parallel$ range.

6. Summary

We have conducted a detailed study of mismatch-induced halo formation from intense spheroidal bunches propagating in a uniform focusing channel. The behavior of axisymmetric linear collective modes is analyzed based on the 3D envelope equations. These fundamental modes turn out to be governed by only three physical quantities, namely, the aspect ratio (or equivalently, the emittance ratio) and the transverse and longitudinal tune depressions. Analytical formulas for the wavenumbers of the breathing and quadrupole-like modes are given as a function of the three basic parameters to explain the power spectra obtained from self-consistent multiparticle simulations.

PIC simulations are performed systematically to reveal how the deviation of an initial beam configuration from the ideal stationary state leads to rms emittance growth and resultant halo formation. The pseudo-equilibrium matching technique is employed to minimize the effect of Debye screening (in other words, self-organization toward an ideal stationary state), which clarifies the emittance growth originating solely from artificial matching errors at injection. We have found that the growth rate is lowered when the degrees of transverse and longitudinal mismatches meet the condition in Eq. (15). At very high beam density, however, a strong mismatch in one direction can enhance halo formation in the other directions through Coulomb coupling. Another practically important finding is that the maximum halo extent scaled with

the maximum rms envelope size depends only weakly upon the degree of initial mismatch. Our PIC data suggest that the aperture radius of a beam pipe should be taken above at least $5a_{\max}$ to prevent halo particles hitting the pipe wall. In the case where $\mu > 1$, $5a_{\max}$ corresponds roughly to $\sqrt{5}\mu$ times the boundary size of the equivalent uniform-density beam.

As repeatedly emphasized in previous papers [7,12,18], we must pay attention to the *full* phase space for correct identification of halo particles. The E-value, an approximate measure for this purpose, is introduced in Section 4 to separate the beam core from the mismatch-induced tail around it. In the case of Fig. 2(b), for instance, less than 20% of the beam particles that have large E-values at injection contribute to the halo observed in Fig. 3(b). The core consisting of the remaining 80% is basically stable even though it executes large coherent oscillation about the matched state. This is a general tendency; a regular mismatch-induced halo is most likely formed from particles with high E-values only. The present PIC data indicate, however, that there exist narrow but dangerous operating regions in which the core stability may be seriously affected. As illustrated in Figs. 9 and 10, severe emittance growth takes place when the parametric resonance conditions in Eqs. (11) are approximately fulfilled.

Acknowledgments

The authors are indebted to Dr K. Kojima for his help and valuable comments in the early stages of this research. This work is supported in part by the Japan Society for the Promotion of Sciences (JSPS) KAKENHI Grant No. 22K12671. Part of the present numerical simulation study was carried out using the computer resources offered by the Research Institute for Information Technology, Kyushu University, under the category of Comprehensive Projects between Hiroshima University and Kyushu University.

References

[1] A. V. Fedotov, AIP Conf. Proc. **693**, 3 (2003).
[2] A. W. Chao and M. Tigner, eds., Handbook of Accelerator Physics and Engineering (World Scientific, Singapore, 1999). doi:10.1142/3818
[3] H. Wiedemann, Particle Accelerator Physics (Springer, Berlin, 1993). doi:10.1007/978-3-662-02903-9
[4] S. Y. Lee, Accelerator Physics (World Scientific, Singapore, 1999). doi:10.1142/3977
[5] K. Kojima, H. Okamoto, and Y. Tokashiki, Phys. Rev. Accel. Beams **22**, 074201 (2019).
[6] K. Kojima, H. Okamoto, and Y. Tokashiki, Phys. Rev. Accel. Beams **23**, 028002 (2020).
[7] H. Okamoto, M. Aoki, C. Ichikawa, K. Kojima, T. Kurauchi, and Y. Yamane, J. Instrum. **15**, P07017 (2020).
[8] H. Okamoto and K. Yokoya, Nucl. Instrum. Meth. A **482**, 51 (2002).
[9] J.-M. Lagniel, Nucl. Instrum. Meth. A **345**, 46 (1994).
[10] R. L. Gluckstern, Phys. Rev. Lett. **73**, 1247 (1994).
[11] T. P. Wangler, RF Linear Accelerators (Wiley, New York, 1998). doi:10.1002/9783527618408
[12] K. Kojima and H. Okamoto, Phys. Rev. Accel. Beams **25**, 024201 (2022).
[13] Y. Yamane, H. Okamoto, and K. Kojima, Phys. Rev. Accel. Beams **24**, 084201 (2021).
[14] J. Qiang, Phys. Rev. Accel. Beams **21**, 034201 (2018).
[15] F. J. Sacherer, IEEE Trans. Nucl. Sci. **NS-18**, 1105 (1971).
[16] J. J. Barnard and S. M. Lund, Proc. Particle Accelerator Conf. (PAC1997), p. 1929 (1997).
[17] J. J. Barnard and S. M. Lund, Proc. Particle Accelerator Conf. (PAC1997), p. 1932 (1997).
[18] H. Okamoto and M. Ikegami, Phys. Rev. E **55**, 4694 (1997).
[19] R. L. Gluckstern, A. V. Fedotov, S. Kurennoy, and R. Ryne, Phys. Rev. E **58**, 4977 (1998).
[20] S. M. Lund, T. Kikuchi, and R. C. Davidson, Phys. Rev. ST Accel. Beams **12**, 114801 (2009).
[21] D. P. Grote, A. Friedman, G. D. Craig, I. Haber, and W. M. Sharp, Nucl. Instrum. Meth. A **464**, 563 (2001).

[22] A. Friedman, R. H. Cohen, D. P. Grote, S. M. Lund, W. M. Sharp, J.-L. Vay, I. Haber, and R. A. Kishek, IEEE Trans. Plasma Sci. **42**, 1321 (2014).
[23] A. V. Fedotov, R. L. Gluckstern, S. S. Kurennoy, and R. D. Ryne, Phys. Rev. ST Accel. Beams **2**, 014201 (1999).